Background-Oriented Schlieren for Large-Scale and High-Speed Aerodynamic Phenomena

Toshiharu Mizukaki[1]
Tokai University, Hiratsuka, Kanagawa, Japan, 259-1292

Stephen Borg,[2] and Paul M. Danehy[3]
NASA Langley Research Center, Hampton, Virginia, 23681,

Scott M. Murman,
NASA Ames Research Center, Moffett Field, CA, 94035

Tomoharu Matsumura,[4] Kunihiko Wakabayashi,[5] and Yoshio Nakayama[6]
National Institute of Advanced Industrial of Science and Technology, Tsukuba, Ibaraki, Japan, 305-8565

Visualization of the flow field around a generic re-entry capsule in subsonic flow and shock wave visualization with cylindrical explosives have been conducted to demonstrate sensitivity and applicability of background-oriented schlieren (BOS) for field experiments. The wind tunnel experiment suggests that BOS with a fine-pixel imaging device has a density change detection sensitivity on the order of 10^{-5} in subsonic flow. In a laboratory setup, the structure of the shock waves generated by explosives have been successfully reconstructed by a computed tomography method combined with BOS.

I. Introduction

Environmental aerodynamic phenomena including sonic boom and wake turbulence are high-speed expanding phenomena which require observation with large fields of view. Researchers have investigated these phenomena with scale-model experiments in laboratories. Model experiments can simulate some Reynolds-number dominated phenomena while others require the use of large scales to capture the physics of interest. The best way to solve these problems is to measure real-scale phenomena in the field.

Several flow visualization methods based on shadowgraph and schlieren have been developed for large-scale experiments including explosions or free flight of high-speed projectiles. Most of these methods are only able to visualize the shape of the shock front. Theoretically, quantitative visualization including interferometry would be possible to carry out in the field. But practically, it is difficult to obtain high-quality interferograms because of strong environmental disturbances including weather, vibrations and background interference.

Background-oriented schlieren (BOS) has been proposed by Raffel[1] and been applied for fluid measurements[2-12] for a decade. The BOS technique uses a background with a randomized pattern and a camera with an imaging lens to visualize the phase object (density disturbance) in front of the background. BOS has two steps: the first is to record a reference image of the background without the density disturbance, the second step is to acquire an image with the density disturbance present. The images are compared using a digital post-processing technique to determine distribution of displacement of the background pattern due to the presence of the phase object. The digital image analysis is based on a cross-correlation analysis similar to that used in particle image velocimetry (PIV). In the case of a two-dimensional or axisymmetric phenomena, the displacement of the background is directly related to the derivative of the density profile of the phenomena in test section. Therefore, BOS has the potential to detect density

[1] Professor, Department of Aeronautics and Astronautics, 4-1, Kitakaname, Senior member AIAA.
[2] Research Engineer, Advanced Measurements and Data Systems Branch, MS 493.
[3] Research Scientist, Advanced Measurements and Data Systems Branch, MS 493, Associate Fellow, AIAA.
[4] Tsukuba Central 5, Chief Research Engineer.
[5] Tsukuba Central 5, Research Engineer.
[6] Tsukuba Central 5, Group Director

profiles of large-scale aerodynamic phenomena propagating at high-speed in the field without the use of lasers or sophisticated optical setups such as interferometers which need fine optical alignment.

In this paper, two kinds of aerodynamic phenomena are visualized by BOS to demonstrate the sensitivity and applicability for field experiments. The shear layer around a generic re-entry capsule model in subsonic flow was conducted to confirm the sensitivity of BOS for a small subsonic wind tunnel test and applications for flight tests. Shock waves generated by explosives with a cylindrical shape were also conducted to explore applicability of BOS for computed-tomography.

II. Background-Oriented Schlieren

Background-Oriented Schlieren (BOS) has been used to visualize the flow density changes for over a decade.[1-11] Its principle of operation is simple and the method is relatively easy to implement with commercial-off-the-shelf equipment. From an optics viewpoint, the BOS method is a white-light speckle photography method that is similar to the laser-speckle method, except that a light source is used instead of a laser. However, from the image-processing viewpoint, the BOS technique uses an image processing method similar to particle image velocimetry (PIV). A significant difference between BOS and PIV is that PIV uses micro-particles, such as oil mist or dust moving with the air, to detect flow. Conversely, the BOS method uses a static background pattern (including random dots) on the other side of the flow from the camera to detect density variations in the air. Minute shifts in the background pattern, due to the density changes in the air, are detected. Thus there is no need to seed the flow with particles.

Another advantage of the BOS method is its unlimited field of view and, consequently, its capacity to monitor objects of unlimited size. Because of the typically conical viewing field of the camera used, the size of any phase object can be matched by changing the distance from the object and the focal length of the camera lens. On the other hand, the conical shape of the projection and different sensitivities of the spatially distributed schlieren necessitate certain correction and calibration procedures. An additional difficulty is the need to focus the background and the object simultaneously. This configuration is achieved by using a small aperture on the camera lens and a short distance between the background and density disturbance, or by using telecentric lenses. Such small apertures require intense illumination. The optimal sensitivity and resolution of the setup are achieved when the background structure has a texture approximately two or three times larger than, the camera resolution.

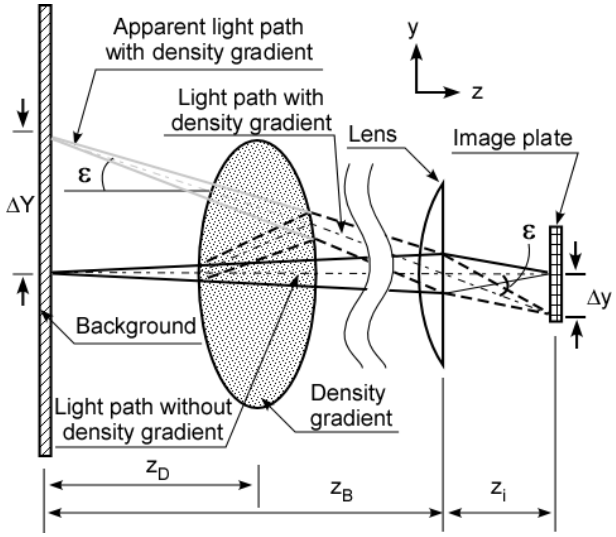

Figure 1. Principle of Background-Oriented Schlieren.

Since the refraction of a single beam contains information about the spatial gradient of the refractive index integrated along the axial path, the image refraction angle ε is defined as[13]:

$$\varepsilon = \frac{1}{n_0}\int_{Z_D-\Delta Z_D}^{Z_D+\Delta Z_D}\frac{\delta n}{\delta y}dZ \tag{1}$$

with the assumption that the half-width of the region of the density gradient $\Delta Z_D << Z_D$. Further, it is seen from the geometry (see Fig. 1) that the virtual image displacement is related to the image displacement by the lens distance

from the background, Z_B, and the image distance from the lens, Z_i , which, for large Z_B, can be replaced by the focal length, f, of the lens:

$$\frac{\Delta Y}{Z_B} = \frac{\Delta y}{Z_i} = \frac{\Delta y}{f} \tag{2}$$

For small deflection angles, ε can be approximated as

$$\Delta y = Z_D M\, \varepsilon \tag{3}$$

where $M = Z_i / Z_B = f/Z_B$. Hence,

$$\varepsilon = \frac{Z_B \Delta y}{Z_D f} \tag{4}$$

The magnitude of the background displacement on the obtained image of the density disturbance (for example, a shockwave) was provided by an image matching algorithm based on the cross-correlation function between the target image and the reference image. After determining the background displacement on imaging device Δy, the refraction angle ε of the light passing through interested phenomenon is determined by equation (3).

III. Experimental setup and Result

A. Subsonic Wind Tunnel Experiment

A capsule model mounted on a sting with an angle of attack at 28 degrees was studied. Figure 2 shows the dimensions of the 4" (101.6 mm) diameter model. The model was installed with the sting horizontal in the test section of the subsonic wind tunnel. The wind tunnel has an octagonal cross section with an inner diameter of approximately 13". Velocities of the main flow were measured with a pitot probe and converted to Mach number. Conditions with Mach 0.20, 0.30, and 0.40 were used.

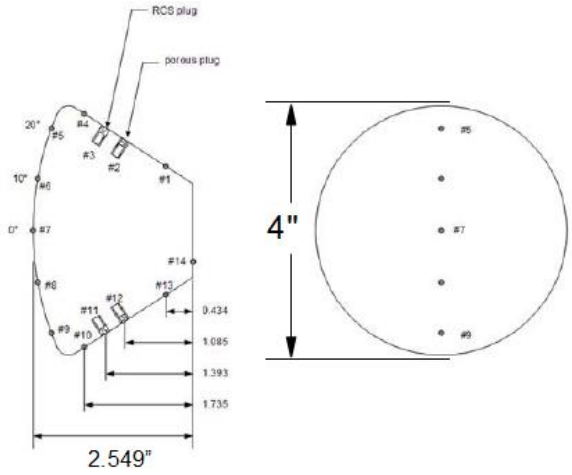

(a) Side view (b) Bottom (Heat shield) –side surface

Figure 2. The generic entry capsule model examined in 13" subsonic wind tunnel.

Figure 3 shows the experimental setup. A random-dot pattern was used as a background, where the diameter and ratio of the black area to the white one was 0.20 mm and 20%, respectively. Reference images, wind-off images, and test images (wind-on) were recorded with the same industrial video camera (Teledyne Dalsa Falcon 2) for one-dimensional density measurements. Flow field images were recorded for one second at a framing rate of 50 Hz and an exposure time of 20 ms for each shot. Background displacement caused by the flow around the model was determined by a cross-correlation analysis with the reference image. In this experiment, the distances from the background to the center of the wind tunnel, Z_B, and to the camera lens, Z_D, were 150 mm and 835 mm. The focal length of the camera lens was 100 mm, and F-number F/22 was chosen.

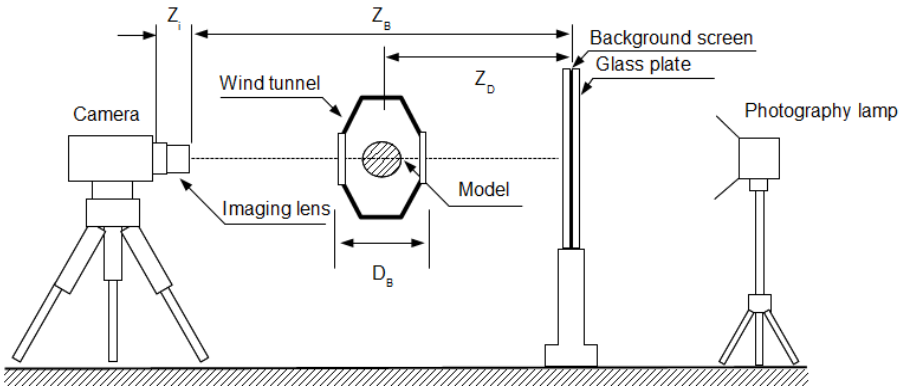

Figure 3. Schematic diagram of visualization setup of BOS for 13" subsonic wind tunnel.

Figure 4 shows maps of background displacement induced by the flow around the capsule model at flow Mach number 0.20, 0.30, and 0.40. The upper row of images represents horizontal pixel displacement toward the right-hand-side and the lower row shows vertical pixel displacement. The colors in the figures indicate background displacement in pixels ranging from -0.5 (blue) to +0.5 (red). In this experiment, negative values of displacement indicate a positive density gradient. On both displacement maps the shear layer, which was emerging from the shoulder of the heat-shield and the back shell of the capsule model toward the downstream, clearly appears in flows with Mach numbers higher than M = 0.3. Also, in front of the capsule model, the expansion region, where the flow was accelerated whilst turning the shoulder from the heat shield to the main flow, is clearly visible. The strength of the expansion region gradually increased in both directions. In Fig. 7, the thickness of the shear layer does not represent the actual thickness because of integrated displacement along the line of sight. The actual shear layer around the capsule model is expected to have oscillation and curvature so that the visualized image shows a thicker shear layer in Fig. 4, which is a consequence of time-integrated blurring. Generally speaking, at lower Mach number, the oscillation amplitude should be larger than that at higher Mach number because of the decreasing oscillation frequency. Therefore, the shear layer in Fig. 4a has a weaker and broader appearance than that in Figs. 4b and c. There is a difference in background color across the upper row of Fig. 4a and b. Theoretically, there should be no displacement in the main flow which would have uniform density distribution. This difference is either the result of an irregular or uniform (DC) background pattern offset caused by unintended movement of the background between runs. Based on the fact that background shift has appeared just in the x-direction between flows at Mach 0.20 and 0.30, some of disturbances originally given by fluid phenomena or the facility have been suspected, but remained unexplained.

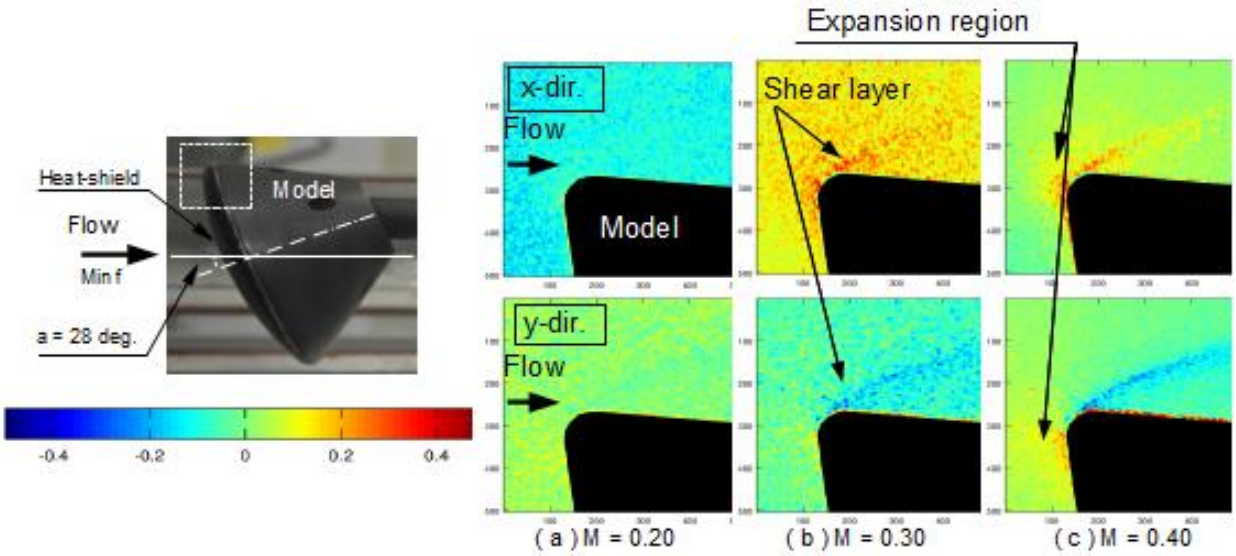

Figure 4. Maps of background displacement on flow Mach numbers ranging from 0.20 to 0.40.

Under the assumption of two-dimensional flow over the measured region, the relative-density difference that was induced by the flow around the capsule model was estimated. Figure 5 shows a horizontal and vertical density change profile across the flow around the capsule model at Mach number 0.4. Figures 5b and 5c show the relative-density-difference profile based on displacement of the background along the broken line X-X' and Y-Y' in Fig.5a. Black dots indicate the density profile is determined by the percentage of atmospheric density on the day of the measurement, 1.258 kg/m^3. The origin of broken lines is at the left-end and the top for X-X' and Y-Y', respectively. Figure 5b shows that a density decrease of about 0.04% from main flow was induced across the shear layer emanating from the shoulder. Figure 5c shows that, in the expansion region in front of the capsule model, a density decrease of about 0.04% was induced.

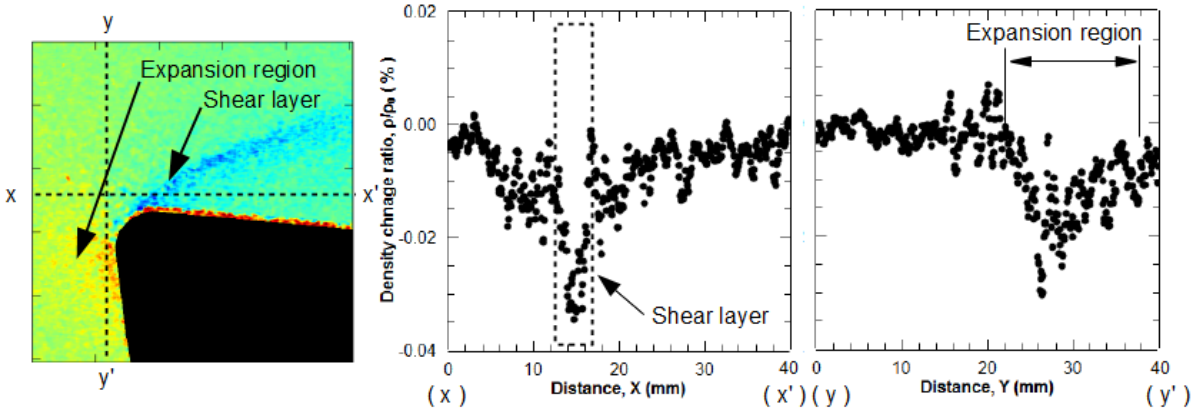

(a) Examined lines (b) Along the line X-X' (c) Along the line Y-Y'

Figure 5. Density profile across the flow field.

Figure 6 shows the density field around the capsule model from the CFD simulation, along with two BOS windows superimposed on the image. The contour lines represent the computed result and the pixel pattern represents the BOS results. In region "A", the shear layer separating from near the maximum diameter of the capsule is clearly visualized by the BOS technique, and qualitatively matches the computational result . Similarly, a small expansion region just upstream of the separation is captured, which also agrees with the computational result. In region "B", the large expansion region developing in front of the heat shield, is clearly visualized with color contour. The shear layer emanating from the marginal region of the heat shield and the side surface is also captured.

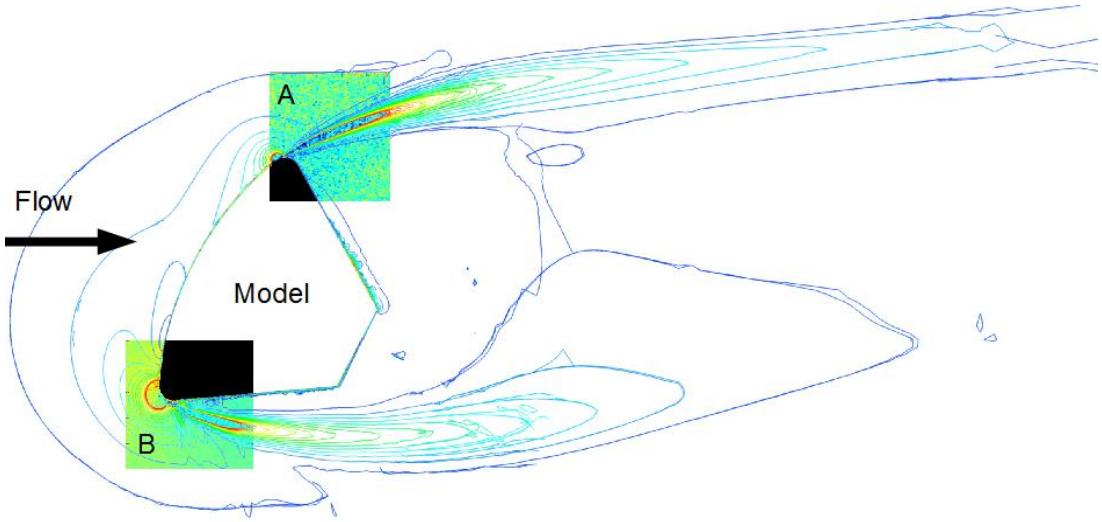

(a)

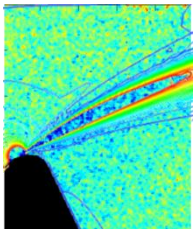

(b)

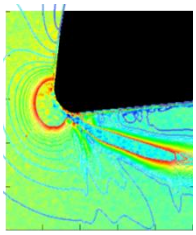

(c)

Figure 6. Comparisons of BOS result with numerical result around the model. a, Superimposed BOS results on the computational result (Global flow field); the BOS results represent background displacement while the computational result density ; **b**, magnification of Region "A"; **c**, magnification of Region "B".

B. The structure of shock waves generated by explosion

Theoretically speaking, shockwaves generated by the instantaneous release of energy in a finite volume has a simple structure which includes spherical shock waves, a so called "negative pressure" region (indicating a relatively low pressure region), and a secondary shock. The incident shock with spherical shape must appear after the release of energy. In the case of using a cylindrical explosive as an energy source to generate the shock wave, however, a distorted shape like a pear will appear because of a strongly oriented combustion jet that propagates from the surface attached to a detonator along the axis of the cylindrical explosive. Therefore, the shock waves generated by pellet-type explosives have non-axisymmetric structure in the early stages of the explosion. After a while, the distorted shape at early stage will be changed to a spherical shape as it propagates over a long distance.

Figure 7 shows schematic diagrams and installation configurations of an asymmetric shock waves being visualized with computed tomography based on BOS. Shock waves, which were generated by small cylindrical explosives, a PETN-pellet with mass of 2-grams (10-mm diameter, 15-mm long), have been visualized by computed tomography based on BOS, herein called CT-BOS. The PETN pellet was ignited with a detonator in the test chamber which has three windows with 30-degree intervals. From each window, a high-speed camera with an imaging lens recorded the propagation of shock waves at 100,000 frames-per-second. The size of the images is 320 by 320 pixels. The high-speed cameras were synchronized to obtain an image sequence from each of the three viewing angles simultaneously. The PETN pellet was installed at the center of the test chamber by attaching a thin, but strong, nylon string under tension. To reconstruct the shock structure, images were recorded from twelve perspectives by rotating the imaging system 3 additional times by 90-degrees.

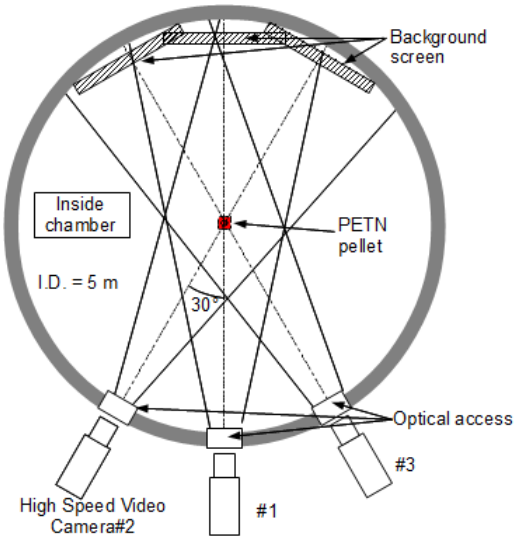

(a) High-speed camera layout (top view)

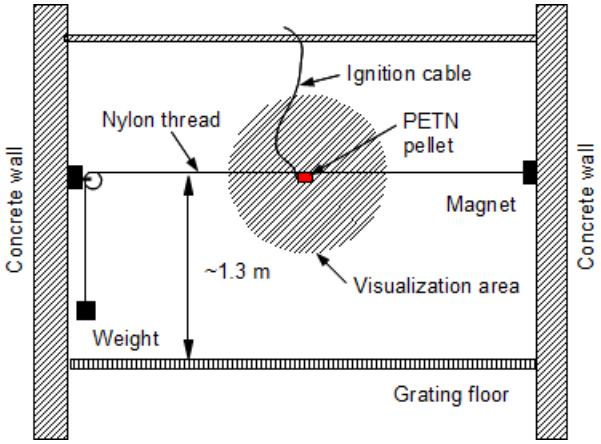

(b) Installation of PETN in the test chamber (side view)

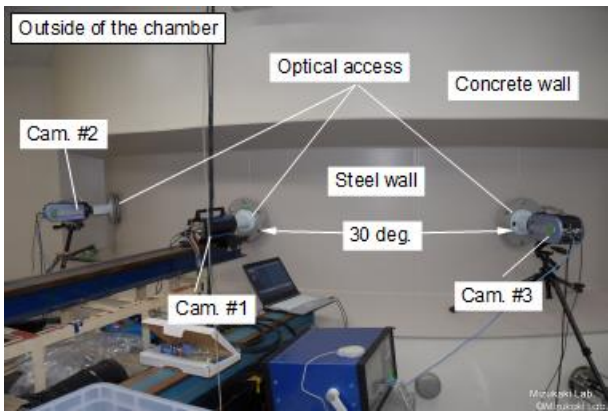

(c) Outside of the test chamber

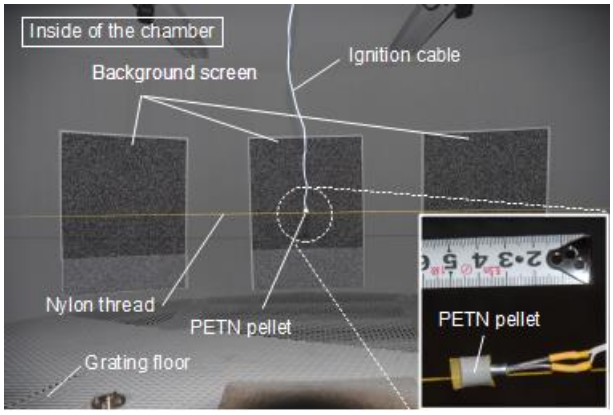

(d) Inside of the test chamber

Figure 7. Schematic diagram of visualization setup of BOS for measuring shock wave structure.

Figure 8 shows the BOS visualization of the shock waves generated by ignition of a PETN pellet. Figure 8a depicts the viewing direction θ of each of the images from twelve directions that have been recorded; only four of the visualizations are shown here. On each figure, the background displacement is shown on the left-hand side, and raw images are shown on the right.

In Fig. 8b, the image obtained from $\theta =$ 0 degrees is shown. From this direction, a spherical shock front appears because the line-of-sight visualization and the axis of PETN pellet attached to the detonator are coincident. Distorted (non-spherical) shocks are propagating toward and away from the observer. In the center of the spherical shock, a relatively dense area is observed where the combustion gas (inside the broken white circle) generated by the explosion of PETN further disturbs the light passing through the shock waves.

Fig. 8c shows the image obtained from θ = 90 degrees. From this direction, a strongly distorted shock wave shape is observed. The PETN pellet was ignited by the detonator from the left-hand side of this image. The detonation wave, which consists of shock waves and combustion waves, propagated from the left side to the right along the pellet's axis. Finally, the detonation wave arrived at the other end of the pellet. At the other side, the propagating detonation wave passed into the air and simultaneously reflected toward the pellet. The reflected wave, which is called an expansion wave, induced negative pressure (vacuum) in the region closest to the pellet. The negative pressure region induced at the opposite surface generates a strong jet which consisted of combustion gas ejected toward the air along the axis. This jet compressed the air to produce a strongly distorted shock wave which propagates to the right-hand side of Fig. 8c.

Fig. 8d shows the image obtained from θ=180 degrees which is similar to Fig. 8b except that the ignited surface is at the opposite end away from the observer. Finally, Fig. 8e shows the image obtained from θ=270 degrees. From this view, the ignited surface is at the right-hand side of the observer.

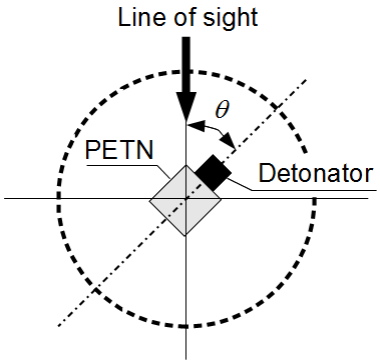

(a) Visualization direction θ

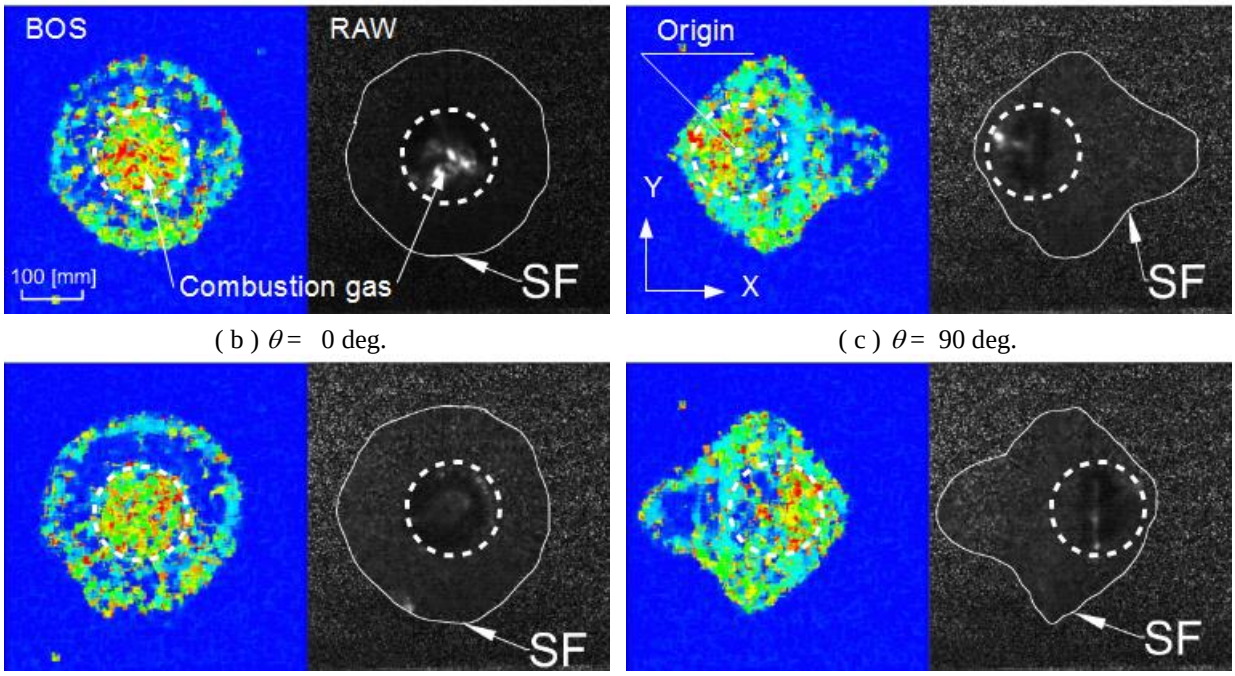

(b) θ = 0 deg.

(c) θ = 90 deg.

(d) θ = 180 deg.

(e) θ = 270 deg.

Figure 8. Analyzed BOS images of explosion with a PETN-pellet from four of twelve directions at 100 μs after ignition; left of (b), (c), (d), and (e), BOS result; right of them, recorded image; SF, shock front.

Figure 9 shows the characteristics of shock front propagation induced by the explosion of the PETN-pellet. The horizontal and vertical distance from the origin of the explosion, which is indicated in Fig. 8c, are plotted in Fig. 9a. In Fig. 9a, the legend X indicates the horizontal direction, and Y the vertical. The subscripts, left/right, and up/down indicate the propagation direction of shock front in each direction. The right bound X_{right} had the fastest propagation velocity among the directions because the combustion gas jet accelerated the shock front while the left bound X_{left} has the lowest velocity. In contrast, both Y_{up} and Y_{down} had similar velocities because of symmetry. The shock front rapidly expanded in all directions until about 100 μs after ignition and then gradually decreased its velocity. From about 200 μs after ignition, the shock front propagated in all directions at the speed of sound, about 340 m/s which is equivalent to 0.034 in Fig. 9b.

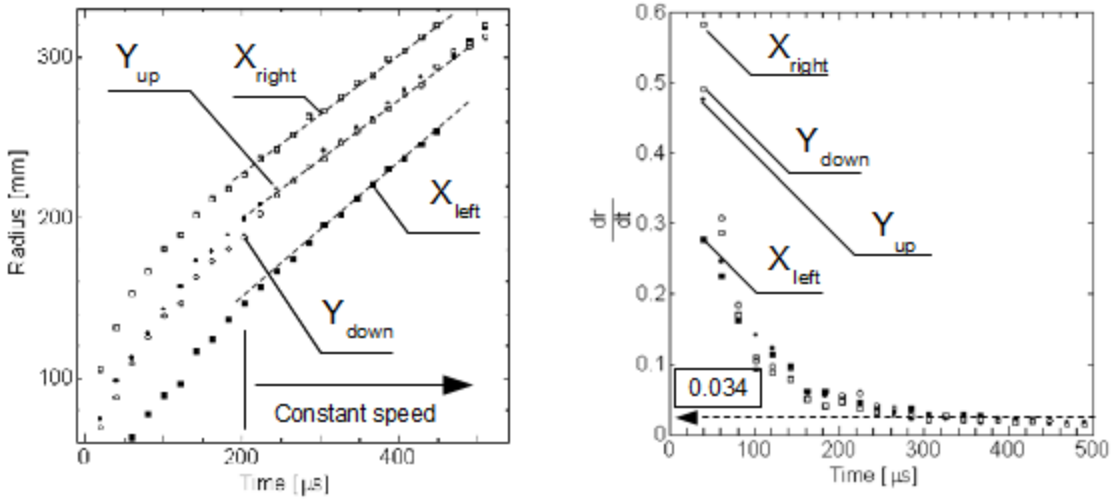

(a) Propagation of the shock front. (b) Expansion rate of the shock front.

Figure 9. Characteristics of shock wave propagation generated by explosion of a PETN-pellet.

Figure 10 shows reconstructed density field inside the shock front by CT-BOS from 50 to 150 μs after ignition. The density field was reconstructed using the algebraic-reconstruction technique (ART)[14] , which is widely used for computed tomography in medical image analysis.[15] . CT-BOS successfully reconstructed the shock-wave structure including the shock front, SF, the combustion gas, CG, and secondary shock, SS. In this experiment, the combustion gas did not allow the background to be seen so that no data were obtained in that region.

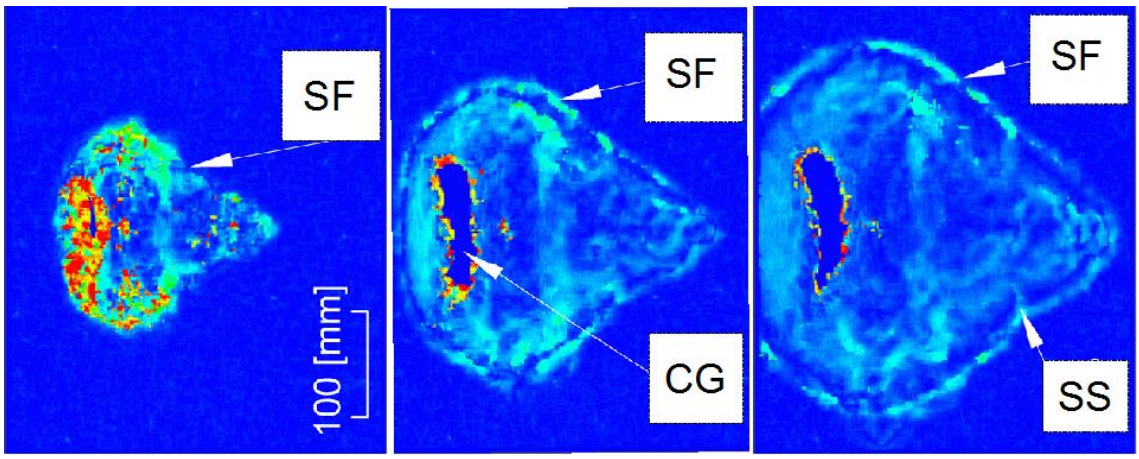

(a) $t = t_0 +$ 50 μs (b) $t = t_0 +$ 100 μs (c) $t = t_0 +$ 150 μs

Figure 10. Background displacement of CT-BOS image of inside the shock front generated by a PETN-pellet ignition. SF, shock front; CG, combustion gas; SS, secondary shock.

V. Conclusion

The background-oriented schlieren (BOS) method was used to visualize the separated flow on the wake of a capsule entry vehicle at low subsonic speed. The flow field around the capsule model was examined in the test section of a subsonic wind tunnel with flow speed ranging from Mach 0.20, 0.30, and 0.40. Both the shear layer emanating from edge of the model and the expansion region in front of the capsule model were clearly visualized by BOS. The shape of these flow structures in the computational simulation agreed qualitatively with measurements at Mach 0.40. This experimental result suggests that BOS has the sensitivity for measuring density variations on the order of 10^{-5} in subsonic flow. This result shows that BOS has the capability of qualitative, and potentially quantitative, visualization

for complicated subsonic flows without the need for particle seeding, toxic gas seeding, or complicated and expensive laser technology.

The BOS technique was also used to reconstruct the structure of propagating shock waves generated by the ignition of a PETN-pellet with mass of 2-grams. From twelve directions, images of the propagating shock waves were recorded by high-speed video cameras. The images were reconstructed by the computed-tomography, algebraic- reconstruction technique (ART) which is widely used in the medical field. The structure of the resulting shock waves were visualized, including the shock front, the secondary shock, and the combustion gas.

References

[1] Richard, H., and Raffel, M. "Principle and applications of the background oriented schlieren (BOS) method," *Measurement Science and Technology* Vol. 12, No. 9, 2001, pp. 1576-1585.

[2] Mizukaki, T., Matsumura, T., Wakabayashi, K., and Nakayama, Y. "Background-oriented schlieren with natural background for quantitative visualization of open-air explosions," *Shock Waves* Vol. 24, No. 1, 2014, pp. 69-78.

[3] Schairer, E., Kushner, L., and Heineck, J. "Measurements of tip vortices from a full-scale UH-60A rotor by retro-reflective background oriented schlieren and stereo photogrammetry," *69th American Helicopter Society Annual Forum*. Phoenix, AZ, 2013, p. Paper #403.

[4] Bauknecht, A., Merz, C., Landolt, A., Meier, A., and Raffel, M. "Blade tip vortex detection in maneuvering flight using the Background Oriented Schlieren (BOS) technique," *69th American Helicopter Society Annual Forum*. Phoenix, AZ, 2013, p. #145.

[5] Venkatakrishnan, L. "Density field measurements of a supersonic impinging jet with microjet control," *AIAA Journal* Vol. 49, No. 2, 2011, pp. 432-437.

[6] Krimse, T., Agocs, J., Schröder, A., Schramm, J. M., Karl, S., and Hannemann, K. "Application of particle image velocimetry and the background-oriented schlieren technique in the high-enthalpy shock tunnel Göttingen," *Shock Waves* Vol. 21, 2011, pp. 233-241.

[7] Mizukaki, T. "Visualization of compressible vortex rings using the background-oriented schlieren method," *Shock Waves* Vol. 20, 2010, pp. 531-537.

[8] Leopold, F. "The application of the colored background oriented schlieren technique (CBOS) to wind tunnel, free-flight and in-flight measurements," *Journal of Flow Visualization and Image Processing* Vol. 16, No. 4, 2009, pp. 279-293.

[9] Hargather, M. J., and Settles, G. S. "Natural-background-oriented schlieren imaging," *Experiments in Fluids* Vol. 48, No. 1, 2009, pp. 59-68.

[10] Sommersel, O. K., Bjerketvedt, D., Christensen, S. O., Krest, O., and Vagsaether, K. "Application of background oriented schlieren for quantitative measurements of shock waves from explosions," *Shock Waves* Vol. 18, No. 4, 2008, pp. 291-297.

[11] Venkatakrishnan, L. "Density measurements in an axisymmetric underexpanded jet by background-oriented schlieren technique," *AIAA Journal* Vol. 43, No. 7, 2005, pp. 1574-1579.

[12] Meier, G. E. A. "New optical tools for fluid mechanics," *8th International Symposium on Flow Visualization*. Sorrento, 1998, p. Paper 226.

[13] Meier, G. E. A. "Computerized background-oriented schlieren," *Experiments in Fluids* Vol. 33, No. 1, 2002, pp. 181-187.

[14] Andersen, A. H., and Kak, A. C. "Digital ray tracing in two-dimensional refractive fields," *J. Acoust. Soc. Amer.* Vol. 72, 1982, pp. 1593--1606.

[15] Herman, G. "Algebraic Reconstruction Techniques," *Fundamentals of Computerized Tomography*. Springer London, 2009, pp. 193-216.